

Alanine Assisted Synthesis and Characterization of $\text{La}_{0.65}\text{Sr}_{0.3}\text{MnO}_3$ (LSM) Nanocrystalline Cathode Powders for Solid Oxide Fuel Cells (SOFCs)

Ghzzai Almutairi^{1,*}, Feraih Alenazey¹, Yousef Yousef¹ and Basheer Alshammari²

¹ Water and Energy Research Institute , KACST, Saudi Arabia

² Petrochemical Research Institute, KACST, Saudi Arabia

*E-mail: gmotair@kacst.edu.sa

Received: 12 June 2017 / Accepted: 14 August 2017 / Published: 12 November 2017

Solid oxide fuel cells (SOFCs) are generally known to be one of the most promising energy conversion devices, offering benefits such as system compactness, high efficiency and low environmental pollution. In this study, $\text{La}_{0.65}\text{Sr}_{0.3}\text{MnO}_3$ (LSM) nanoceramic powders were prepared through the citrate-nitrate auto-combustion route with a β -alanine-to-nitrate ratio of 1:1. Thereafter, a Thermolyne 47900 furnace was used to calcine the prepared powders at 900 °C for 4 hrs to remove carbonaceous residues, and then, the prepared powders were characterized using SEM/EDS, XRD, and TGA. Calculations using the Debye-Scherrer equation illustrated that the average crystallite size of the powders was approximately 20-25 nm. There was no loss in weight after reaching a temperature of ~700 °C, as indicated by TGA, signifying the completion of combustion. Electrochemical characterization of the $\text{La}_{0.8}\text{Sr}_{0.2}\text{MnO}_3$ (LSM) cathode powders was performed by coating these powders (as the cathode functional layer (CFL) with 40-60 wt% 8YSZ on the bottom and the catalyst layer (CL) on the top) using the screen printing technique on SOFC half-cells (NiO-YSZ+YSZ) obtained from CGCRI (Kolkata, India) with a cell size of 36 mm dia \times 1.6 mm (effective electrode area of ~1.13 cm²). These cells were tested with H₂ and O₂ at 750-800 °C with flow rates of 1.2-1.8 lit min⁻¹ H₂ and 0.4-0.6 lit min⁻¹ O₂ with a hydrogen humidification of 3%. The current density (cd) and power density (pd) were the highest for the CFL containing 60 wt% LSM and 40 wt% YSZ. The cd and pd of the single SOFC cell were 0.8 A cm⁻² (at 0.7 V) and 0.6 W cm⁻², respectively, at 800 °C, a hydrogen flow rate of 1.8 lit min⁻¹ and an oxygen flow rate of 0.6 lit min⁻¹.

Keywords: Strontium-doped lanthanum manganite, Solid Oxide Fuel Cell, Nickel anode, Ytria-stabilized zirconia, Cathode functional layer, Current collector layer

1. INTRODUCTION

Significant attention has been given to solid oxide fuel cells (SOFCs) over the last three decades due to their high efficiency (~80% including thermal), fuel flexibility, and potential

environmental advantages [1, 2]. However, the high cost involved has been a hindrance to the commercialization of SOFC technology, thereby necessitating the development of superior materials to enable the design of more economically viable systems. $\text{La}_{0.8}\text{Sr}_{0.2}\text{MnO}_3$ (LSM) is recognized as a classical cathode material for SOFC-based yttria-stabilized zirconia electrolytes, because it possesses excellent thermal properties, a high electrical conductivity, chemical stability and band compatibility with ZrO_2 -based electrolytes at working temperatures of 800-1000 °C. The cathode for O_2 reduction is also a crucial area for SOFC development since the cathode polarization commonly dominates the performance of these cells; as this reaction primarily occurs at lower operating temperatures, inexpensive materials can be used in the construction of SOFC components. LSM powders can be produced by several methods, such as electrochemical synthesis, solid-phase synthesis, and sol-gel methods [3-5]. Presently, the design of the SOFC cell unit is based on a yttria-stabilized zirconia (YSZ) solid electrolyte and electrodes consisting of Sr-doped LaMnO_3 (cathode) and Ni-YSZ cermet (anode) [6,7]. Though LSM is an excellent cathode material for high-temperature SOFCs due to its high catalytic activity towards oxygen reduction, good stability and excellent compatibility with YSZ electrolytes, LSM is less efficient at lower cell operating temperatures (700-800 °C) due to its low ionic and electronic conductivity, resulting in a drastic reduction in active sites beyond the three-phase-boundary [8,9].

In modern years, some researchers [10,11] have attempted to enhance the SOFC cell performance by using $\text{La}_{0.65}\text{Sr}_{0.3}\text{MnO}_3$ with 50 wt% YSZ as a cathode functional layer. In an attempt to study the electrical, thermal and electrochemical properties at 600-800 °C, Pal et al. [10] prepared $\text{La}_{0.65}\text{Sr}_{0.3}\text{MnO}_3$ with an L-alanine-to-nitrate ratio of 1:1 using an auto-ignition process. Haanappel et al. [11] studied the optimization of the microstructural and processing parameters of LSM cathodes to enhance the performance of anode-supported SOFCs. The best density attained at present is 1.5 A cm^{-2} at 0.7 V with a LSM:YSZ ratio of 50:50 by weight at 800 °C. Buchkremer et al. [12] reported that a double-layered $\text{La}_{0.65}\text{Sr}_{0.3}\text{MnO}_3$ (LSM)/LSM- Y_2O_3 -stabilized ZrO_2 (YSZ) cathode applied on a thin YSZ layer could be operated between 800-1000 °C. The best density attained was 0.5 A cm^{-2} at 750 °C and 0.7 V.

This investigation seeks to study the performance of $\text{La}_{0.65}\text{Sr}_{0.3}\text{MnO}_3$ cathode powders in SOFC cells that are 36 mm in diameter. This study uses a cathode functional layer (CFL) with 50 wt% $\text{La}_{0.65}\text{Sr}_{0.3}\text{MnO}_3$ and 50 wt% YSZ or 60 wt% $\text{La}_{0.65}\text{Sr}_{0.3}\text{MnO}_3$ and 40 wt% YSZ and utilizes CL ($\text{La}_{0.65}\text{Sr}_{0.3}\text{MnO}_3$) as the current collector layer (top layer). A study of the electrochemical characteristics of the above powders was performed in SOFC single cells at 700-800 °C using H_2 and O_2 in a uniquely designed and fabricated fuel cell test station, and the collected data were employed to draw I-V and I-P curves.

2. EXPERIMENTAL PROCEDURE

2.1 Preparation of $\text{La}_{0.65}\text{Sr}_{0.3}\text{MnO}_3$ (LSM-1) Nanoceramic Powders:

The $\text{La}_{0.65}\text{Sr}_{0.3}\text{MnO}_3$ (LSM-1) nanoceramic powders were prepared using the auto-combustion technique [13-14] with the applicable and required amounts of $\text{La}(\text{NO}_3)_3 \cdot 6\text{H}_2\text{O}$ (BDH), $\text{Sr}(\text{NO}_3)_2$, $\text{Mn}(\text{CH}_3\text{COO})_2 \cdot 4\text{H}_2\text{O}$, citric acid (BDH) and distilled water. The preparation of the precursor solution

involved mixing individual aqueous solutions of the above chemicals with 99.0% purity. The required citric acid was then added to all of the nitrate solutions and mixed properly until a clear solution was formed in the Pyrex glass without any precipitation.

The β -alanine-to-nitrate ratio was maintained at 1:1. To evaporate the solution, the Pyrex glass beaker was heated on a hot plate at 250 °C using a magnetic stirrer until a gel was formed. After further heating, the gel was completely incinerated, resulting in the creation of a light, fragile ash. Thereafter, a Barnstead Thermolyne 47900 Furnace (USA) was used to calcine the ash at 900 °C for 4 hrs. Figure 1 shows the flow sheet for the preparation of the LSM powders by the auto-ignition technique.

In the present study, two types of cathodes were studied. The first (cell # 220) consists of 50 wt% LSM and 50 wt% YSZ (10-15 μm) as the cathode functional layer (CFL-1) and LSM-1 as the cathode layer (CL), which is a 30 μm top layer. The cathode of cell # 222 consists of 60 wt% LSM and 40 wt% YSZ (10-15 μm) as the cathode functional layer (CFL-2) and LSM-1 as the cathode layer (CL), which is a 30 μm top layer.

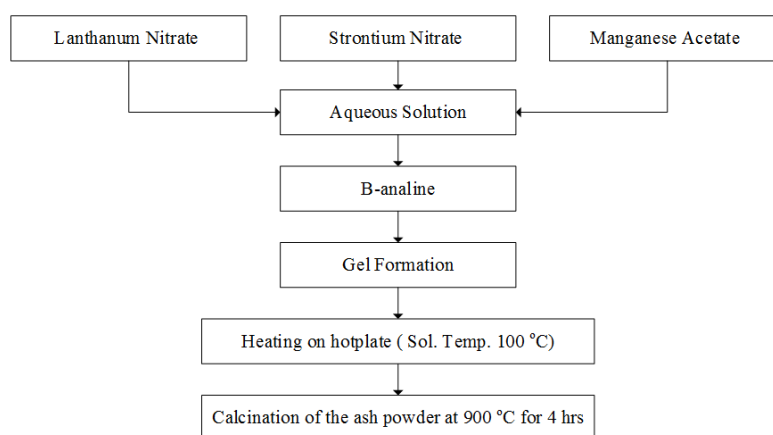


Figure 1. Flow sheet for preparing $\text{La}_{0.65}\text{Sr}_{0.3}\text{MnO}_3$ cathode nano ceramic powder by auto-ignition technique.

2.2 Physical Characterization:

Physical characterizations, such as scanning electron microscope (SEM), energy dispersive X-ray spectroscopy (EDS), X-ray diffraction (XRD), thermal gravimetric analysis (TGA) and surface area analysis, were used to characterize the LSM samples. These physical characterization techniques were described in our previous works [15,16].

2.3 Electrochemical Characterization:

2.3.1 SOFC Half-cells (36 mm dia x 1.5 mm) procured from CGCRI, Kolkata, India

NiO-YSZ +YSZ half-cells (16 mm dia \times 1.5 thick) were commercially procured from CGCRI (Kolkata, India). The anode (NiO-YSZ) had a thickness of 1.5 mm, and the electrolyte (YSZ) had a

thickness of approximately 15 microns. The tape casting technique was used to fabricate the half-cells (NiO-YSZ-YSZ) to produce the electrolyte (YSZ) and anode (NiO-YSZ) layers. These were then laminated and pressed at room temperature, and both the electrolyte and anode were consequently co-sintered at 1400 °C for 6 hrs at a rate of 1 °C hr⁻¹. Details of the electrode fabrication (half-cells) process are available in the references [17, 18].

2.3.2 Preparation of cathode functional layer (CFL) and cathode layer (CL) pastes

The milled powders of the cathode functional layer (CFL) containing 50 wt% cathode layer (CL) and 50 wt% YSZ or 60 wt% cathode layer (CL) and 40 wt% YSZ and the cathode layer (CL) were weighed separately and prepared as pastes for application in the half-cells. Using tissue paper, isopropyl alcohol/acetone was used to wipe the cleaned agate bowl and grinder. Then, 10 gr of the cathode active layer powder CFL-1 and 10 gr of the catalyst powder LSM were separately placed in two agate mortars with 2 gr of ethyl cellulose as a binder and 20-25 drops of terpinol as a thinner and mixed thoroughly for 2 hrs to yield a homogeneous paste. The thinner (terpinol) was added every 30 minutes. The two pastes were collected into two small bottles. CFL-2 with 60 wt% CL and 40 wt% YSZ was prepared in a similar manner.

2.3.3 Screen printing of the CFL and CL layers on the NiO-YSZ half-cells

One 10-15 micron layer (the CFL-1 layer) was first printed over the yttria-stabilized zirconia (YSZ) surface of the half-cell and then dried for half an hour. Then, 3 layers (~30-35 microns) of the La_{0.8}Sr_{0.2}MnO₃ cathode paste were applied over the dried CFL-1 layer using a screen printer produced by SKYHILL Ming Tai Screen Printing Machine Co., Ltd. (China). After the screen printed half-cells were dried, they were collected in a dense alumina plate, covered with another plate and placed in a furnace. They were then sintered at 1050 °C for 4 hrs from room temperature to 600 °C (1 hr) at 75 °C hrs⁻¹, up to 1050 °C at 100 °C hrs⁻¹ and then cooled to room temperature at 150 °C hrs⁻¹. At this stage, the full cell was ready for testing in a fuel cell test station. Similarly, CFL-2 and CL layers were applied on other half-cells/single cell components.

2.3.4 Description of experimental set-up for testing 36mm dia SOFC Cells and assembly

The experimental setup for testing the 36 mm diameter SOFC cells reported by other researchers is similar to the SOFC test stations and configurations of this research [19, 20]. A brief overview of the test station and scheme of the SOFC single-cell assembly are presented in the previous work [16].

3. RESULTS AND DISCUSSION

3.1 Physical Characterization

3.1.1 SEM / EDX

Figure 2 shows the SEM images of the calcined and milled LSM powders. The oxide particles are observed to be well crystallized, with clear shapes and particle diameters of less than 300 nm [21]. Thereafter, the powders were milled for 24 hrs using ethanol as the medium with ZrO₂ balls 5 mm in diameter. They were then dried at 100 °C to prepare the CFL before application in the 36 mm diameter half-cells.

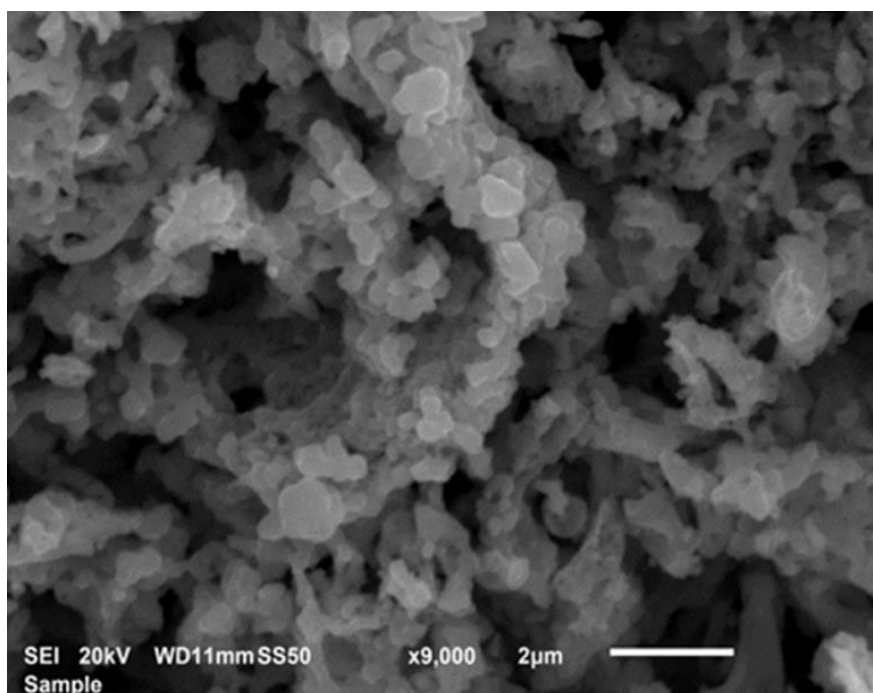


Figure 2. SEM of La_{0.65}Sr_{0.3}MnO₃ [LSM] powders calcined at 900 °C 4 hrs⁻¹

Figure 3 shows the SEM image of the CFL powder after milling for 24 hrs using ZrO₂ balls 5 mm in diameter. A fine structure is evident in the diagrams, with particles of less than 150 nm and slight agglomeration.

The EDS plots of the LSM powders at two different spots/areas together, indicating the qualitative amounts of elements in the powders, are shown in Figures 4a-4b. From the EDS analysis (Table 1) of the LSM powders, it is noted that the components have slightly different atomic ratios.

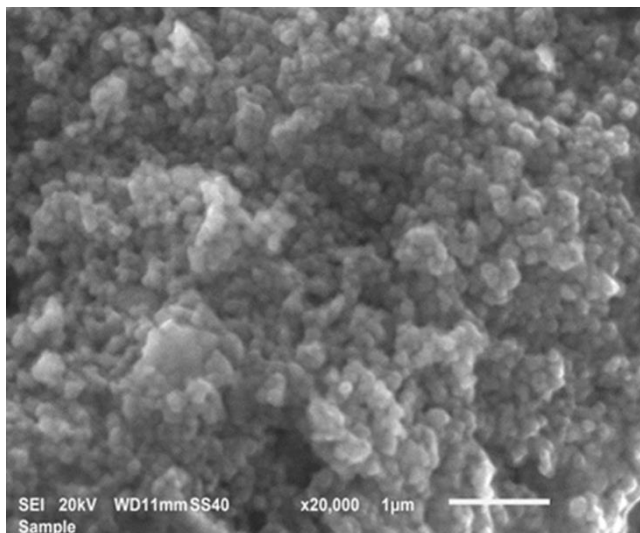


Figure 3. SEM of CFL powder [50% LSM-50% YSZ] milled for 24 hrs.

Table 1. Results of EDS analysis of LSM powders

Component	Weight %			Atomic %			Atomic ratio		
	La	Sr	Mn	La	Sr	Mn	La	Sr	Mn
La _{0.65} Sr _{0.3} MnO ₃ [Calcined] Spot-1	51.1	17.2	31.6	32.28	17.2	50.4	0.64	0.34	1.00
La _{0.65} Sr _{0.3} MnO ₃ [Calcined] Spot-2	50.3	18.0	31.5	31.7	18.0	50.2	0.63	0.36	1.00

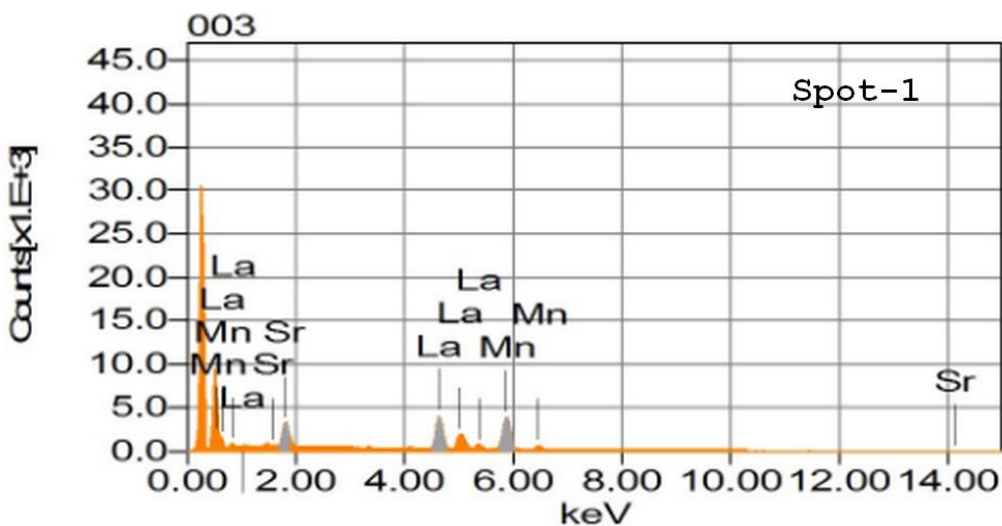


Figure 4. a: EDS pattern of LSM powder calcined at 900 °C 4 hrs⁻¹ at Spot-1

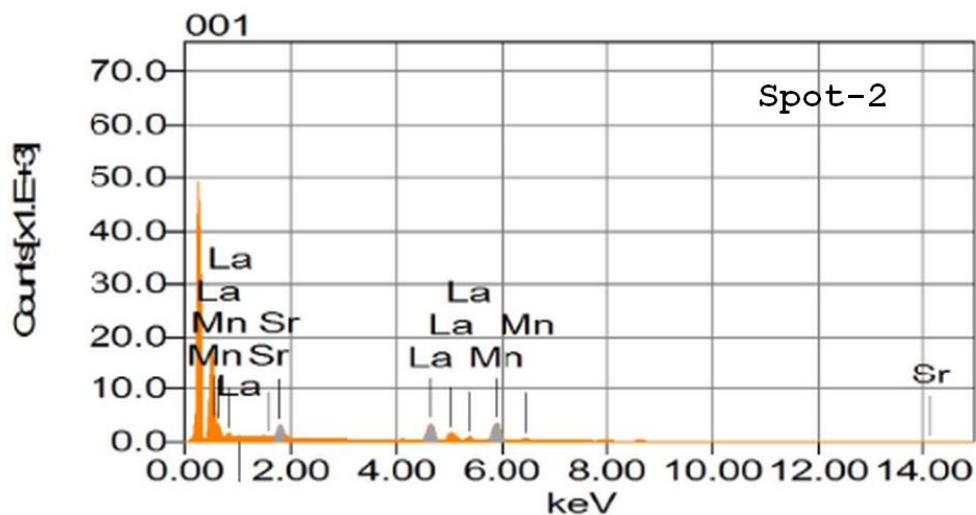


Figure 4. b: EDS pattern of LSM powder calcined at 900 °C 4 hrs⁻¹ at Spot-2

3.2 TGA Characterization

Figure 5 shows the thermal gravimetric analysis (TGA) of the as-prepared LSM nanopowders in the range of 30-900 °C. Three clear stages of weight loss can be observed. The initial weight loss of adsorbed water occurred at 160 °C, signifying the decomposition of the lanthanum-alanine and manganese-alanine complexes and the formation of the crystalline phase of the pure LSM powder. The TGA plot of LSM shows a drastic weight loss at ~250 °C. After reaching a temperature of ~600-650 °C, no further weight loss is observed in the TGA plots, which indicates the completion of combustion. Notably, the thermal behaviour of the LSM powders in this research is comparable with that of LSM powders reported elsewhere [22, 23].

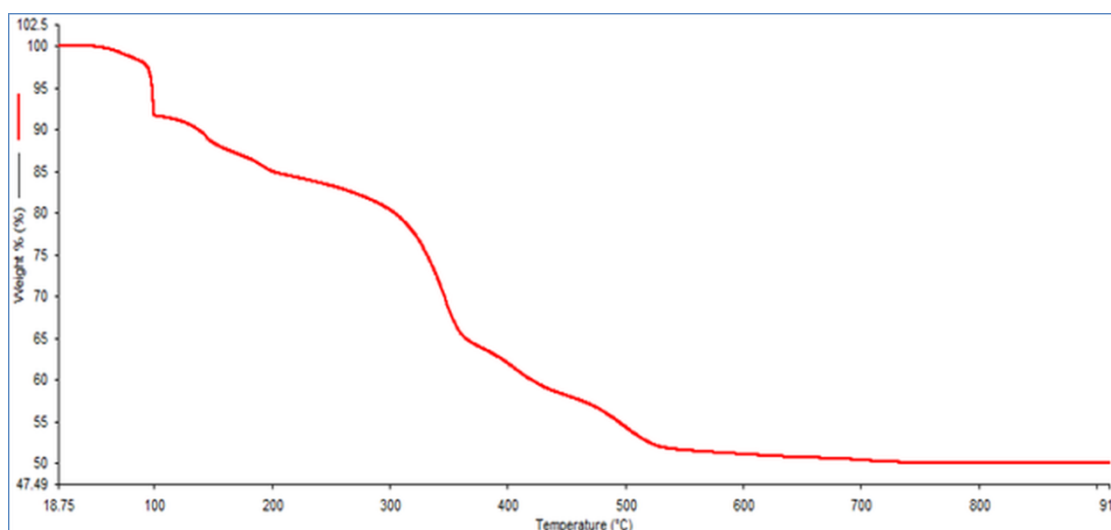


Figure 5. TGA Plot of LSM -245 (as prepared) powder #245

3.3 XRD Characterization

The XRD patterns of the LSM powders are demonstrated in Figures 6 and 7, showing the as-prepared powder and that calcined at 900 °C for 4 hrs⁻¹. The calcined powder was milled for 24 hrs in isopropanol medium. The obtained peaks resemble those reported by other authors [24]. The XRD data in Table 2 gives the crystallite size of the LSM powders to be 16.46 nm and 19.43 nm for the as-prepared and sintered LSM powders, respectively. The powder obtained after calcination at 900 °C was pure and is very similar with the outcomes of similar studies [25]. Table 3 shows that the crystallite size of the calcined powders is slightly higher than that of the as-prepared powders.

Table 2. XRD data to determine the average crystallite size of the LSM powders

Sample ID Number	Cos θ	With CuK α Radiation λ (Co) = 0.15418nm	
		B FWHM	Crystallite size, t (nm)
245a [LSM] As prepared powder	Cos15.19	0.5012	16.46
245 b [LSM] (Calcined at 900°C / 4hrs)	Cos15.19	0.42469	19.43

Avg. crystallite size = $t = 0.9 \times \lambda / B \cos \theta$, B= FWHM in $^\circ$, $B = [FWHM \times 22/7 \div 180] = FWHM \times 0.017460$

Table 3. Average crystallite size of LSM powders

Sample ID Number	Surface Area(m ² /g) Multipoint BET	Average crystallite size with $d_{BET} = 6 / [d_{th} \times S_{BET}]$ [20, 25] nm	Average crystallite size with XRD d_{XRD} , nm	d_{BET} / d_{XRD}
245a [LSM]	24.30	37.55	16.46	2.28
245b [LSM]	21.50	42.80	19.43	1.99

D_{BET} = average crystallite e size, d_{th} = theoretical density of LSM (6.521 gr cc⁻¹), S_{BET} = surface area (m² gr⁻¹)

The average particle size d_{XRD} of the as-prepared powders was 16.46 nm, whereas a d_{XRD} of 19.43 nm was identified for the calcined powders. These values were acquired from the available XRD data using the Debye-Scherrer equation. These d_{BET} and d_{XRD} values are comparable with the findings of previous studies [23].

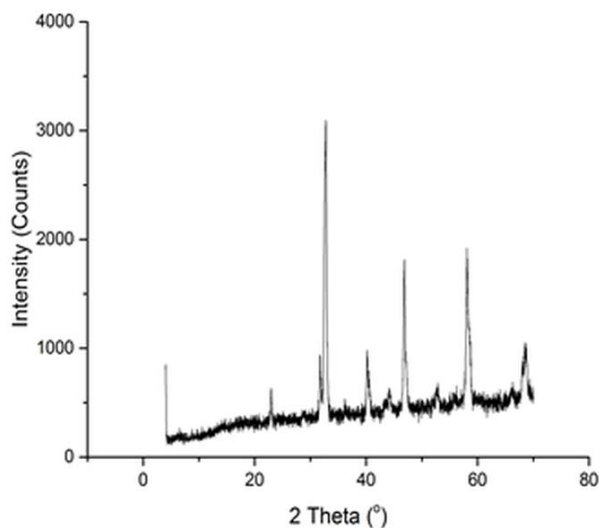


Figure 6. XRD patterns of LSM-245a powder (as prepared)

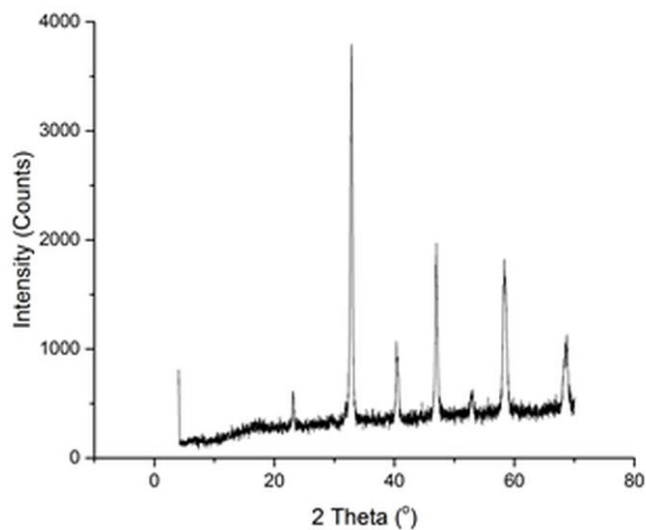


Figure 7. XRD patterns of LSM-245b powder calcined at 900 °C

3.4 Electrochemical Characterization of SOFC Single Cell

Figures 8a-8c show the I-P and I-V curves for a single SOFC cell [# 220] with a cathode functional layer of 50 wt% LSM and 50 wt% YSZ with three hydrogen (1.2-1.8 lit min⁻¹) and oxygen (0.4-0.6 lit min⁻¹) flow rates at three operational temperatures (700, 750, 800 °C) using 3% humidified hydrogen gas. The OCV values of the cells were in the range of approximately 1.08-1.09 V, indicating a dense structure with a well-formed electrolyte layer on the NiO-YSZ surface, meaning that leakage is insignificant. As illustrated in Figure 8a, the maximum current density (cd) obtained is approximately 0.7 A cm⁻² at a cell voltage of 0.7 V, and the power density (pd) is approximately 0.53 W cm⁻² at 800 °C, with H₂ and O₂ flow rates of 1.2 lit min⁻¹ and 0.4 lit min⁻¹, respectively. However, reduction of the cell operating temperature to 750 °C and 700 °C reduces the cd values to 0.53 A cm⁻² and 0.4 A cm⁻²,

respectively. Additionally, the pd values decreased to 0.35 W cm^{-2} at $750 \text{ }^\circ\text{C}$ and 0.30 W cm^{-2} at $700 \text{ }^\circ\text{C}$. This decrease is attributable to the low temperatures, as their obtained area specific resistance (ASR) increased to $0.65\text{-}0.91 \text{ } \Omega \text{ cm}^2$, which is slightly higher than the accepted value (\sim less than $0.5 \text{ } \Omega \text{ cm}^2$) for SOFC applications.

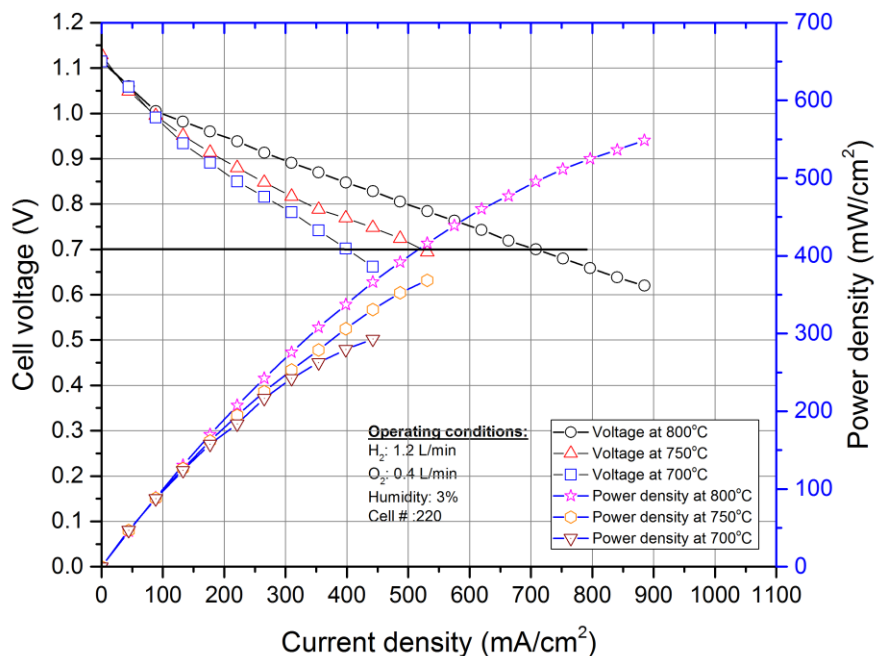


Figure 8a. I-V and I-P curves of Cell #220 with different temperatures ($700\text{-}800 \text{ }^\circ\text{C}$) at flow rates (1.2 H_2 and $0.4 \text{ O}_2 \text{ lit min}^{-1}$) with cathode functional layer: $50 \text{ wt}\% \text{ LSM} + 50 \text{ wt}\% \text{ YSZ}$.

Figure 8b shows the I-V and I-P curves for the single SOFC cell [# 220] with the flow rates of 1.5 lit min^{-1} for hydrogen and 0.5 lit min^{-1} for oxygen at temperatures ranging from $700\text{-}800 \text{ }^\circ\text{C}$ with the same 3% humidified hydrogen gas. As shown in Figure 11b, the maximum current density obtained is approximately 0.75 A cm^{-2} , which occurs at a cell voltage of 0.7 V and power density of approximately 0.60 W cm^{-2} at $800 \text{ }^\circ\text{C}$. The cd and pd values are noted increase slightly by increasing the gas flow rates of 1.5 lit min^{-1} for hydrogen and 0.5 lit min^{-1} for oxygen. Similar results were observed when the cell operating temperatures were reduced to $750 \text{ }^\circ\text{C}$ and $700 \text{ }^\circ\text{C}$, at which the cd and pd values fell to 0.55 A cm^{-2} and 0.40 W cm^{-2} (at $750 \text{ }^\circ\text{C}$) and 0.45 A cm^{-2} and 0.33 W cm^{-2} (at $700 \text{ }^\circ\text{C}$).

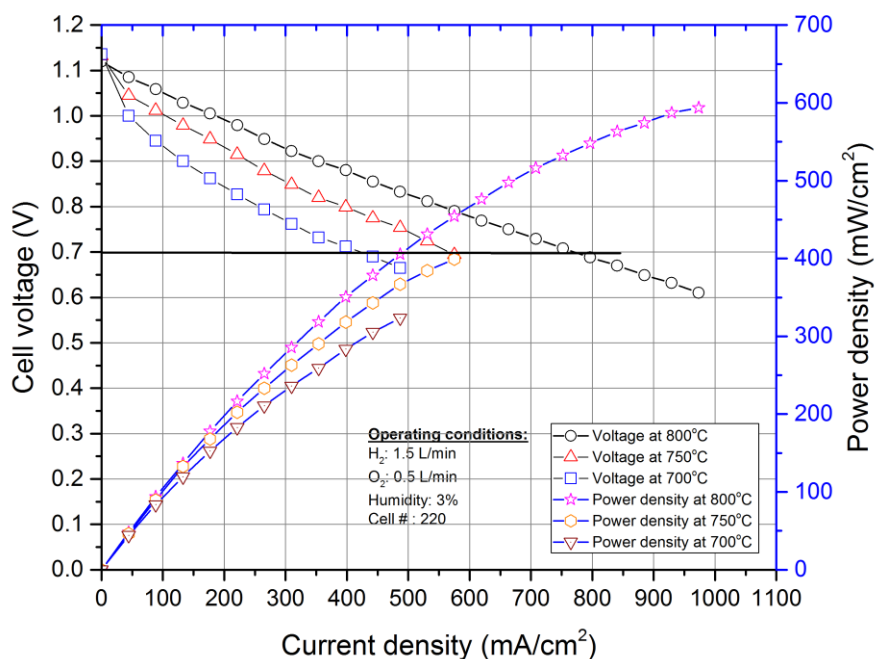


Figure 8b. I-V and I-P curves of Cell #220 with different temperatures (700-800 °C) at flow rates (1.5 H₂ and 0.5 O₂ lit min⁻¹) with cathode functional layer: 50 wt% LSM + 50 wt% YSZ.

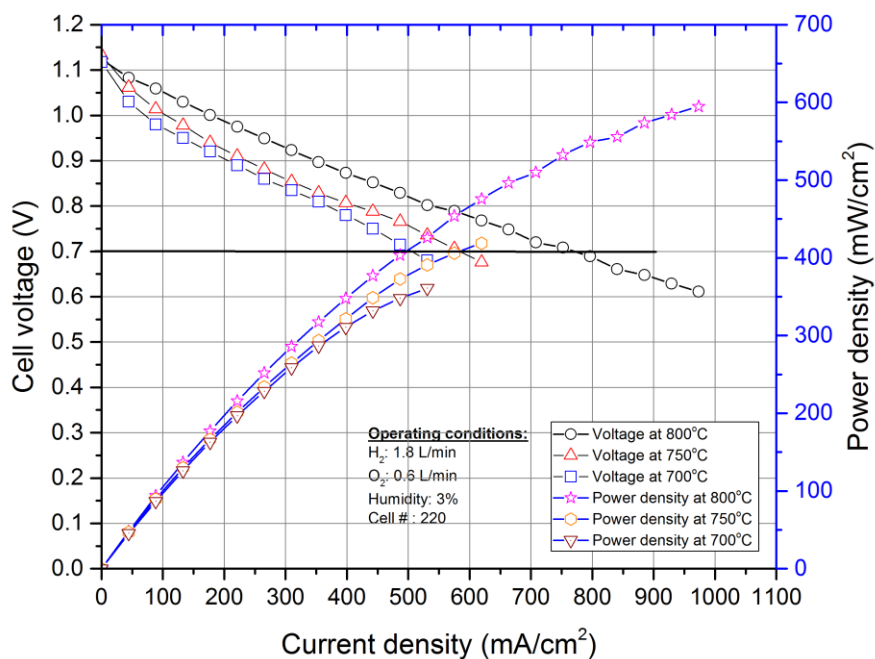


Figure 8c. I-V and I-P curves of Cell #220 with different temperatures (700-800 °C) at flow rates (1.8H₂ and 0.6 O₂ lit min⁻¹) with cathode functional layer: 50 wt% LSM + 50 wt% YSZ.

Figure 8c shows the I-V and I-P curves for a single SOFC cell [# 220] with the flow rates 1.8 lit min⁻¹ hydrogen and 0.6 lit min⁻¹ oxygen at 700-800 °C with the same 3% humidified hydrogen gas. Figure 8c shows that the maximum current density obtained is approximately 0.76 A cm⁻² at a cell voltage of 0.7 V, and the power density is approximately 0.60 W cm⁻² at 800 °C. However, by reducing the cell operating temperature to 750 °C and 700 °C, the cd and pd values decreased to 0.58 A cm⁻² and 0.4 W cm⁻² and 0.40 A cm⁻² and 0.35 W cm⁻², respectively. An increase in the flow rates results in a slight increase in the pd and cd values.

Figures 9a-9c show the I-V and I-P curves for the single SOFC cell [# 222] with a cathode functional layer containing 60 wt% LSM and 40 wt% YSZ with at three hydrogen (1.2-1.8 lit min⁻¹) and oxygen (0.4-0.6 lit min⁻¹) flow rates at three operating temperatures (700, 750, 800 °C) using 3% humidified hydrogen gas. The OCV values of the cells were approximately 1.08-1.09 V, signifying that a dense structure electrolyte formed on the NiO-YSZ surface, ensuring that the leakage is insignificant. Figure 9a shows that the maximum current density (cd) attained is approximately 0.77A cm⁻² at a cell voltage of 0.7 V, and the power density (pd) is approximately 0.58 W cm⁻² at 800 °C with H₂ and O₂ flow rates of 1.2 lit min⁻¹ and 0.4 lit min⁻¹, respectively. However, a reduction in the cell operating temperature to 750 °C and 700 °C lowers the cd and pd values to 0.65 A cm⁻² and 0.50A cm⁻² and 0.5 W cm⁻² and 0.35 W cm⁻², respectively. The resulting low temperatures reduced the reaction rates, as the ASR values increased to 0.0.603-0.753 Ω cm², which are slightly higher than the accepted values (~less than 0.5 Ω cm²) for SOFC applications.

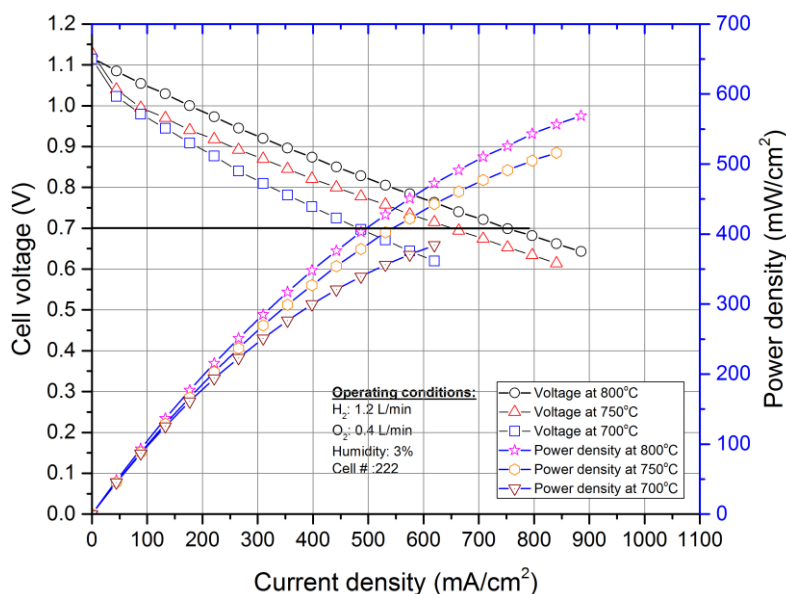


Figure 9a. I-V and I-P curves of Cell #222 with different temperatures (700-800 °C) at flow rates (1.2H₂ and 0.4 O₂ lit min⁻¹) with cathode functional layer: 60 wt% LSM + 40 wt% YSZ.

Figure 9b shows that the maximum current density (cd) reached approximately 0.8 A cm⁻² at a cell voltage of 0.7 V and a power density (pd) of approximately 0.61 W cm⁻² at 800 °C with H₂ and O₂ flow rates of 1.5 lit min⁻¹ and 0.5 lit min⁻¹, respectively. The ASR value was 0.469 Ω cm².

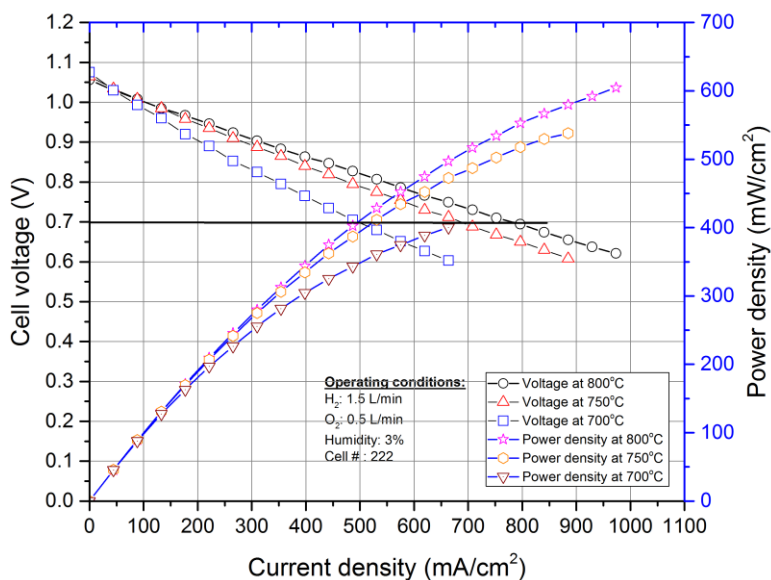


Figure 9b. I-V and I-P curves of Cell #222 with different temperatures (700-800 ° C) at flow rates (1.5H₂ and 0.5 O₂ lit min⁻¹) with cathode functional layer: 60 wt% LSM + 40 wt% YSZ.

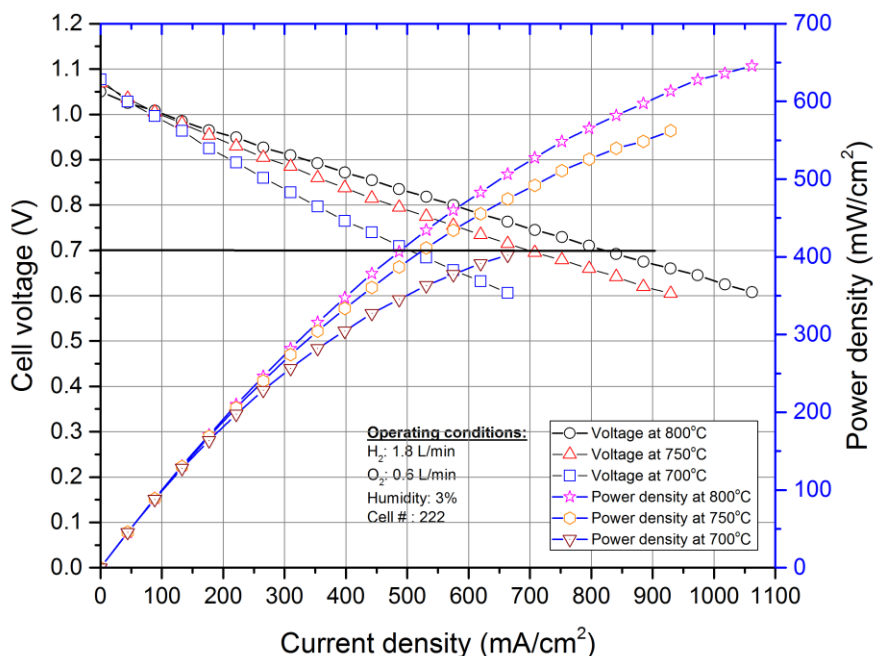


Figure 9c. I-V and I-P curves of Cell #222 with different temperatures (700-800 ° C) at flow rates (1.8H₂ and 0.6 O₂ lit min⁻¹) with cathode functional layer: 60 wt% LSM + 40 wt% YSZ.

Figure 9c shows the I-V and I-P curves for the single SOFC cell [# 222] with flow rates of 1.8 lit min⁻¹ for hydrogen and 0.6 lit min⁻¹ for oxygen at 700-800 ° C with the same 3% humidified

hydrogen gas. Figure 9c shows that the maximum current density obtained is approximately 0.85 A cm^{-2} at a cell voltage of 0.7 V , and the power density is approximately 0.65 W cm^{-2} at $800 \text{ }^\circ\text{C}$. Reduction of the cell operating temperature to $750 \text{ }^\circ\text{C}$ and $700 \text{ }^\circ\text{C}$ reduces the cd and pd values to 0.70 A cm^{-2} and 0.55 W cm^{-2} and 0.50 A cm^{-2} and 0.38 W cm^{-2} . It is noted that an increase in the flow rates only causes a slight increase in the current density and power density values. The above figures clearly indicate that lowering the YSZ content in cathode functional layer to $40 \text{ wt}\%$ enhances the performance, proposing the potential use of such materials for intermediate SOFC applications.

The results from this study support those of earlier studies [19, 26]. Other reasons may exist for lowering the cd and pd, such as fuel starvation and reduced reaction kinetics at the cathode, especially at low temperatures (approximately $700\text{-}750 \text{ }^\circ\text{C}$). Therefore, special cathode materials, such as CGO/LSCF, and different anode functional layers should be developed to attain a higher output power at lower temperatures $\sim 700 \text{ }^\circ\text{C}$, as reported by Moon et al. [26].

Tables 4 and 5 show the summary of the results of the current density, power density and linear plots of the ASR values at temperatures of $700\text{-}800 \text{ }^\circ\text{C}$ for a CFL composed of $50 \text{ wt}\%$ LSM and $50 \text{ wt}\%$ YSZ or $60 \text{ wt}\%$ LSM and $40 \text{ wt}\%$ YSZ. The ASR values are lower for the CFL composed of $60 \text{ wt}\%$ LSM and $40 \text{ wt}\%$ YSZ. The ASR values obtained from the linear portion of the I-V curves show a relatively low resistance loss at different operating temperatures. The values obtained ($\sim 0.432 \text{ } \Omega \text{ cm}^2$) at 0.7 V and $800 \text{ }^\circ\text{C}$ in the present work are quite comparable with those reported elsewhere [28, 29]. This supports the assertion that such cells may be viable cathode materials for use in low-temperature ($800 \text{ }^\circ\text{C}$) SOFC applications. The factors of the anode side that affect the performance of the single cell include its microstructure, three-phase boundary, pore/pore size distribution, anode electrolyte interference, and anode thickness. The parameters that result in cell voltage loss at a given operational current density include activation/concentration, polarization of the electrode and Ohmic polarization of the electrolyte/anode interference.

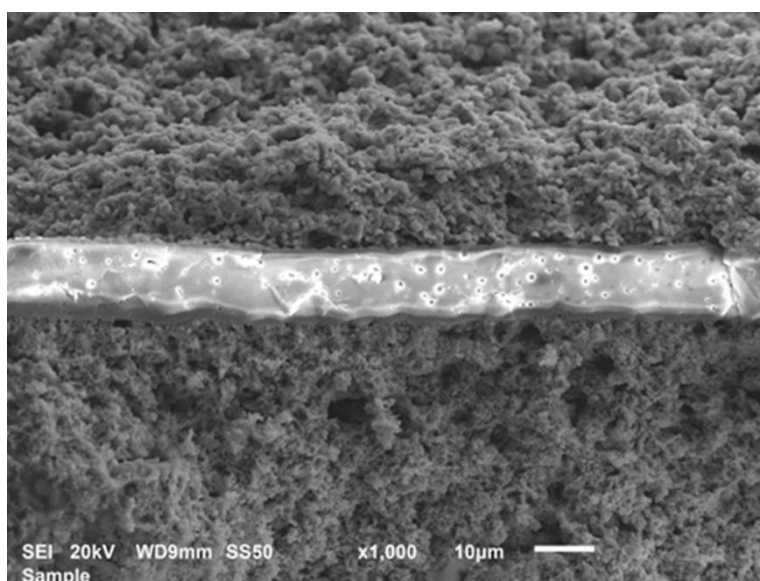
Table 4. Area specific resistance values calculated from the linear portion of the I-V curves at different temperatures for Cell # 220

Flow rates (L min^{-1})	Operating Temp. $^\circ\text{C}$	Current density mA cm^{-2}	Power density mW cm^{-2}	ASR $\Omega \text{ cm}^2$
H_2 : 1.2 O_2 : 0.4	700	400	300	0.908
	750	510	368	0.770
	800	707	548	0.650
H_2 : 1.5 O_2 : 0.5	700	442	323	0.790
	750	575	400	0.730
	800	780	595	0.602
H_2 : 1.8 O_2 : 0.6	700	490	361	0.708
	750	580	420	0.690
	800	790	600	0.590

Table 5. Area specific resistance values calculated from the linear portion of the I-V curves at different temperatures for Cell # 222

Flow rates (L min ⁻¹)	Operating Temp. °C	Current density mA cm ⁻²	Power density mW cm ⁻²	ASR Ω cm ²
H ₂ : 1.2 O ₂ : 0.4	700	480	380	0.753
	750	640	516	0.563
	800	750	585	0.603
H ₂ : 1.5 O ₂ : 0.5	700	510	400	0.751
	750	685	538	0.541
	800	796	612	0.469
H ₂ : 1.8 O ₂ : 0.6	700	530	410	0.640
	750	707	562	0.544
	800	810	650	0.432

Figure 10 presents an SEM micrograph of the anode surface and a cross section of the SOFC single cell, showing the various CL and CFL layers of NiO-YSZ and YSZ. The ~12 micron YSZ electrolyte is supported by the anode, which has a thickness of 1.5 mm. The YSZ layer was dense and uniform, with no open pin holes and a continuous and crack-free surface morphology, and the cathode and anode layers were both well-adhered to the electrolyte layer. Figure 9c (Cell #222) clearly shows that the CFL composed of 60 wt% LSM and 40 wt% YSZ gave a higher power output due to the lower resistance. By decreasing the thickness of the CL layer and introducing an anode functional layer, as presented by Moon et al. [26], it may be possible to obtain even better performance for the SOFC cells. The results of the present study support those reported previously by other authors [27, 29].

**Figure 10.** SEM micrographs of anode surface and cross section of SOFC Single Cell after testing at 800 °C.

4. CONCLUSIONS

The findings of the current work enable the following conclusions to be drawn:

1. The LSM nanoceramic powders were prepared by the auto-ignition technique with a β -alanine-to-nitrate ratio of 1:1, with an average crystallite size of 15-16 nm. The Debye-Scherrer equation and the SEM images indicate that particle size of the LSM powders is ~200-300 nm.
2. The LSM powders were shown to have surface areas of $23.4 \text{ m}^2 \text{ gr}^{-1}$ and $21 \text{ m}^2 \text{ gr}^{-1}$ for the as-prepared and calcined powders, respectively.
3. The XRD patterns show the formation of the pure LSM powders after calcination of the ash obtained by auto-ignition at $900 \text{ }^\circ\text{C}$ for 4 hrs.
4. The TGA plots of the as-prepared LSM powders show that no weight change occurs after $600 \text{ }^\circ\text{C}$, indicating the completion of combustion.
5. The CFL with 50 wt% YSZ worked satisfactorily to achieve a current density of 0.8 A cm^{-2} at 0.7 V and power density of 0.6 W cm^{-2} with a H_2 flow rate of 1.8 lit min^{-1} and an O_2 flow rate 0.6 lit min^{-1} . However, by increasing the LSM content to 60 wt% CFL, the cd increased to 0.85 A cm^{-2} at 0.7 V, and the highest power density was measured to be 0.65 W cm^{-2} at $800 \text{ }^\circ\text{C}$. This indicates that such materials could be applicable in intermediate-temperature SOFC applications.
6. The values obtained for the ASR were $0.43\text{-}0.55 \text{ } \Omega \text{ cm}^2$ at 0.7 V and $800 \text{ }^\circ\text{C}$ with a H_2 flow rate of 1.8 lit min^{-1} and an O_2 flow rate of 0.6 lit min^{-1} for 36 mm diameter SOFC cells.

References

1. Q. Minh, *Solid State Ionics*, 174 (2004) 271-277.
2. J. Molenda, K. Swierczek, W. Zajac, *Journal of Power Sources* 173 (2007) 657-670.
3. M. Gaudon, C. Laberty-Robert, F. Ansart, P. Steven, A. Rousset, *Solid State Science*, 4 (2002) 125-133.
4. M Ghouse, Y. Alyousef, A. Al Musa, M. Alotaibi, *Intentional Journal of Hydrogen Energy*, 35 (2010) 9411-9419.
5. M. Aparicio, A. Jitianu, L. Klein *Sol-Gel processing for Conventional & Alternative Energy*, Springer: New York, 2012. Chendong Z, Mingfei L, Meilin L. *Solid Oxide Fuel Cells*, 1 (2012) pp 7- 36.
6. J. Huo, H. Uanderson, *Solid State Chemistry*, 87 (1990) 55 -63.
7. P. Decorse, G. Caboche, C. Dufour, *Solid State Ionics*. 117 (1991) 161.
8. C. Singhal, *Solid State Ionics*. 152 (2002) 405-410.
9. P. Jiang, *Solid State Ionic*., 146 (2002)1-22.
10. P. Pal, W. Raja, J. Mukhopadhyay, *ECS Transaction*., 7 (2007) 1129-1138.
11. A. Haanapple, D. Rutenbeck, A. Mai, *Journal of Power Source*. 130 (2004) 119-128.
12. P. Buchkremer, U. Dieckmann, D. Stover, in *Proceedings of the Second European Solid Oxide Fuel Cell Forum, Oslo, Ulf Bossel*, May 1996: p.221
13. R. Basu, S. Pratihar, M. Saha, *Materials Letters*. 32 (1997) 217-222.
14. A. Chakraborty, P. Devi, H. Maiti, *Proc. The 4th Inter. Sym.on Solid Oxide Fuel Cell, Yokohoma, Japan*, June 1995: 18-23.
15. G. Almutairi, M. Ghouse, Y. Alyousef, *Journal of New Materials for Electrochemical Systems* 2016 2.

16. G. Almutairi, Y. Alyousef, F. Alenazey, S. Alnassar, H. Alsmail, M. Ghouse, *International Journal of Electrochemical Science* 11 (2016).
17. R. Basu, A. Das Sharma, A. Dutta, *International Journal of Hydrogen Energy*, 20 (2008) 5748-5754.
18. R. Basu, A. Das Sharma, A. Dutta, *Energy*. 7 (2007) 227-234.
19. S. Kim, H. Moon, S. Hyun, J. Moon, J. Kim, H. Lee, *Solid State Ionics*, 177 (2006) 931-938
20. J. Song, S. Park, H. Jong, *Journal of Materials Processing Technology*. 198 (2008) 414-418.
21. J. Wang, K. Ta, J. Shao, *Journal of Power Source*,. 186 (2009) 344-348.
22. A. Dutta, J. Mukhopadayaay, R. Basu, *Journal of the European Ceramic Society*. 29 (2009) 2003-2011.
23. S. Ghosh, S. Dasgupta, *Materials Science-Poland*. 28 (2010) 421-438.
24. www.intechopen.com/<http://cdn.intechopen.com/pdfs-wm/36185.pdf>- page392
25. R. Moriche, D. Marrero-Lopez, F. Gotor, *Journal of Power Sources*.252 (2014) 43-50.
26. H. Moon, S. Kim, H. Hyun, *International Journal of Hydrogen Energy*. 33 (2008) 1758-1768.
27. S. Kim, H. Hyun, J. Moon, *Journal of Power Sources*. 139 (2005) 67-72.
28. Z. Wang, J. Qian, J. Cao, S. Wang, T. Wen, *Journal of Alloys and Compounds* 437 (2007) 264-268.
29. V. Haanapple, J. Mertens, D. Rutenbeck, C. Tropicartz, W. Herzhof, D. Sebold, F. Tietz, *Journal of Power Sources*, 141 (2005) 216-226.

© 2017 The Authors. Published by ESG (www.electrochemsci.org). This article is an open access article distributed under the terms and conditions of the Creative Commons Attribution license (<http://creativecommons.org/licenses/by/4.0/>).